J. Chem. Sci. Vol. 125, No. 4, July 2013, pp. 895–903.

Quasi-classical trajectory study of the reaction $N(^4S) + H_2$ and its reverse reaction: Role of initial vibrational and rotational excitations in chemical stereodynamics

JUAN ZHANG and SHUNLE DONG*

College of Information Science and Engineering, Ocean University of China, Qingdao 266071, China
e-mail: dongshunle2013@hotmail.com

MS received 29 June 2012; revised 26 September 2012; accepted 6 November 2012

Abstract. To investigate the effects of reagent vibrational and rotational states on the stereodynamical properties of the $N(^4S) + H_2(v, j) \rightarrow NH + H$ reaction and its reverse reaction of $H(^2S) + NH(v, j) \rightarrow N(^4S) + H_2$, we reported a detailed quasiclassical trajectory study using the $^4A''$ double many-body expansion potential energy surface and at the collision energy of 35 kcal/mol. The density distribution of $P(\theta_r)$ as a function of the angle between $\boldsymbol{k}$ and $\boldsymbol{j'}$, and that of $P(\varphi_r)$ as a function of the dihedral angle between the plane containing $\boldsymbol{k}$–$\boldsymbol{k'}$ and the plane containing $\boldsymbol{k'}$–$\boldsymbol{j'}$, the normal differential cross-sections as well as the averaged product rotational alignment parameter $\langle P_2(\boldsymbol{j'} \cdot \boldsymbol{k}) \rangle$ are calculated and reported. Comparison between the two reactions has showed that the degrees of alignment and orientation of products related to reagent rovibrational state have marked differences for the two reactive systems.

Keywords. Stereodynamics features; vibrational excitation; rotational excitation; quasiclassical trajectory calculation.

1. Introduction

Reactions involving the nitrogen atom are of essential importance to atmospheric chemistry and combustion chemistry. While reactions of electronically excited $N(^2D)$ with H_2 have been widely studied,[1–4] some research attention has been paid to $N(^4S) + H_2 \rightarrow NH + H$ and its reverse reaction. Theoretically, for the $NH(X^3\Sigma^-) + H \rightarrow N(^4S) + H_2$ reaction, Xu *et al.*[5] depicted the energy profiles along the intrinsic reaction coordinate (IRC) and reported its potential barrier at the MP-SAC4/6-311G level. In the temperature range 2000–3000 K, their calculated variational- transition-state rate constants agree well with the experimental values. Using a direct *ab initio* dynamics method, Zhang and Truong[6] studied the kinetics of the $N(^4S) + H_2 \rightarrow NH(^3\sum^-) + H$ reaction at the QCISD(TQ)/cc-pVTZ level, providing information on reaction path, forward and reverse barriers, energies along the minimum energy path, etc. They also calculated thermal rate constants with the microcanonical variational transition state theory. In 2002, Pascual *et al.*[7] reported a detailed quasiclassical trajectory (QCT) and variational transition state theory study of the two reactions, employing their own constructed potential energy surface (PES) at the MCQDPT2// FORS-MCSCF(7,6)/6-311++G** level. They found that the $NH + H(^2S) \rightarrow N + H_2$ reaction prefers a product vibrational level of $v' = 1$ for trajectories initiated at low translational energy of E_T. Moreover, their calculated rate constants for the forward and reverse reactions were in good accord with available experimental and theoretical data. Recently, Han *et al.*[8] reported the total reaction cross-section, the averaged product rotational alignment parameter of the reverse reaction initiated from the ground vibrational-rotational state of the reactants. They found that the specific vibrational-rotational rate constant showed an Arrhenius-type behaviour over the investigated temperature range of 200–2500 K, in excellent agreement with the experimentally available data. Experimentally, Koshi *et al.*[9] presented the rate constant expression of $(2.8 \pm 0.2) \times 10^{14} \exp(-(33 \pm 7)/RT)$ for the $N(^4S)+H_2 \rightarrow NH+H$ reaction. He also calculated the activation energy which is in good agreement with the experimental measurement. Using atomic resonance absorption spectrophotometry (ARAS), Davidson and Hanson[10] reported the first direct measurement of the rate coefficient for the reaction $N(^4S) + H_2 \rightarrow NH + H$. In 2005, Adam *et al.*[11] determined the room temperature rate coefficient for the reaction $NH + H(^2S) \rightarrow N(^4S) + H_2$, and this measurement agrees well with the

*For correspondence

rate coefficient from the QCT calculation on the global potential energy surface for the $^4A''$ state.

Though many researchers have explored the $N(^4S)+H_2$ and NH + $H(^2S)$ reaction involving the $^4A''$ electronic state, existing information about the chemical stereodynamics of these two reactions, especially the role that the reagent vibrational and rotational excitations played in their chemical stereodynamics, is rather sparse. In order to understand the dynamics of the two reactions fully, we apply the QCT method to these two reactions initiated from different rovibrational states for the purpose of studying the polarization of product rotational angular momentum, discussing the influence of the initial reagent rovibrational states on the product vector properties, as well as comparing the stereodynamics characters between $N(^4S) + H_2$ and its reverse reaction.

The PES[12–19] provides information about the interaction of a reactive system at a molecular level and thus plays a significant role in kinetics and dynamics studies. In the present study, we employed the single-sheeted double many-body expansion (DMBE) PES by Poveda and Varandas.[14]

The next section describes concisely the calculation method. The penultimate section presents the results and discussion; the final section concludes the article.

2. Theory

The QCT calculation method is the same as that mentioned in references[20–30]. Figure 1 shows the centre-of-mass (CM) coordinate system utilized in the present QCT calculation, where the z-axis is parallel to the reagent relative velocity $\boldsymbol{k}$, the product relative velocity $\boldsymbol{k'}$ is contained in the xz plane, while the y-axis is perpendicular to the xz scattering plane. θ_t is called the scattering angle, representing the angle between the reagent relative velocity and product relative velocity. θ_r and φ_r are the polar and azimuthal angles of the product rotational angular momentum $\boldsymbol{j'}$.

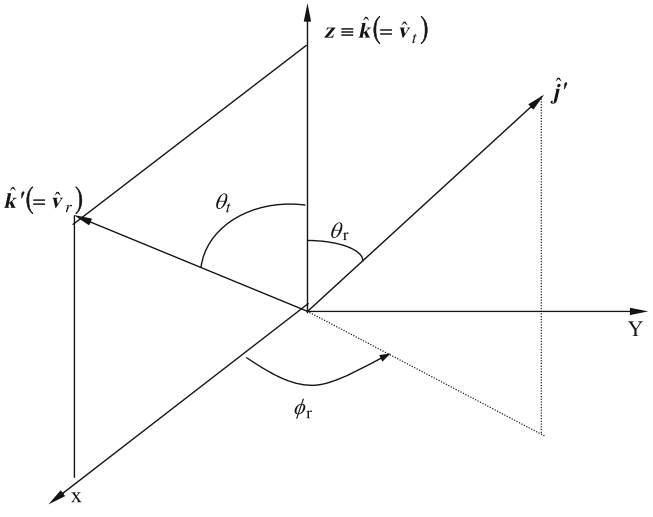

Figure 1. The centre of mass frame used in the QCT calculation and the description of the vectors and their correlations.

The distribution function $P(\theta_r)$, which describes the $\boldsymbol{k} - \boldsymbol{j'}$ correlation, can be expanded in a series of Legendre polynomials,[31–33]

$$P(\theta_r) = \frac{1}{2}\sum_k (2k+1)\, a_0^k\, P_k(\cos\theta_r)\,, \qquad (1)$$

where

$$a_0^k = \langle P_k(\cos\theta_r)\rangle\,.$$

Here the angular brackets represent an average over all the reactive trajectories.

The dihedral angle distribution function $P(\varphi_r)$, which describes the $\boldsymbol{k} - \boldsymbol{k'} - \boldsymbol{j'}$ correlation, can be written as,[31,32]

$$P(\varphi_r) = \frac{1}{2\pi}\left[1 + \sum_{n\ \text{even}\ \geq 2} a_n \cos(n\varphi_r) + \sum_{n\ \text{odd}\ \geq 1} b_n \sin(n\varphi_r)\right], \qquad (2)$$

where $a_n = 2\langle\cos n\varphi_r\rangle$ and $b_n = 2\langle\sin n\varphi_r\rangle$.

The generalized polarization-dependent differential cross-section ($PDDCS_{00}$)[32] is given by,

$$\frac{2\pi}{\sigma}\frac{d\sigma_{00}}{d\omega_t} = P(\omega_t) = \frac{1}{2}\sum_{k_1}[k_1]\, h_0^{k_1}(k_1,0)\, P_{k_1}(\cos\theta_t)\,, \qquad (3)$$

where the bipolar moments $h_0^{k_1}(k_1,0)$ are evaluated using the expected value expression,

$$h_0^{k_1}(k_1,0) = \left\langle P_{k_1}(\cos\theta_t)\right\rangle. \qquad (4)$$

It is noted that $\frac{d\sigma_{00}}{d\omega_t}$ in the left hand side of (3) is just the normal differential cross-section that can be experimentally measured. Thus, in the following section, we obtained this normal differential cross-section from $PDDCS_{00}$ by dividing a factor of $2\pi / \sigma$.

In our calculations, the trajectories are run on the single $^4A''$ electronic state, which means that the present QCT investigation does not consider the nonadiabatic dynamics[34–42] of the system arising from the Renner–Teller effect and other nonadiabatic coupling terms. In order to investigate the initial rovibrational excitation effects on product polarizations, we choose the reagent vibrational levels of $v = 1, 3, 5, 7$ when $j = 0$ and rotational levels of $j = 2, 4, 6, 8$ when $v = 0$ in our QCT calculations. The collision energy is chosen to be 35 kcal/mol, and the initial distance from the N atom to

Table 1. The optimized maximum impact parameters for each reaction initiated from different v, j values.

Reactions rovibrational state	$v=0$ $j=0$	$j=0$ $v=1$	$j=0$ $v=3$	$j=0$ $v=5$	$j=0$ $v=7$	$v=0$ $j=2$	$v=0$ $j=4$	$v=0$ $j=6$	$v=0$ $j=8$
N (^{4}S) + H_2 → NH + H	0.9	1.42	1.95	2.37	2.75	0.96	0.9	1.05	1.25
H (^{2}S) + HN → H_2 + N	2.28	2.55	2.98	3.35	3.75	2.29	2..28	2.28	2.33

the centre of mass of H_2 is 15 Å. Batches of 10,000 trajectories are run for each rovibrational state. The integration step size is chosen as 0.1 fs to ensure the conservation of total energy and total angular momentum. The optimized maximum impact parameter for each rovibrational state is listed in table 1 for N(^{4}S) + H_2 → NH + H and its reverse reaction.

3. Results and discussion

3.1 *Effects of vibrational excitation on N(^{4}S) + H_2 and its reverse reaction*

The distribution of $P(\theta_r)$ for the two systems shown in figure 2 reflects the $\boldsymbol{k} - \boldsymbol{j'}$ correlation of the products with $\boldsymbol{j'} \cdot \boldsymbol{k} = \cos\theta_r$. As seen, the two reactions illustrate symmetric distributions peaked at $\theta_r = 90°$, which implies that product rotational angular momentum vector $\boldsymbol{j'}$ strongly aligns along the perpendicular direction to $\boldsymbol{k}$. In detail, in figure 2(a), the $P(\theta_r)$ distribution becomes higher and narrower with the increasing initial vibrational quantum number, as revealed in the $v = 0$, 1 and 3 cases. However, at higher vibrational states such as $v = 5$ and 7, products exhibit a weaker tendency of being aligned along the direction perpendicular to the reagent relative velocity $\boldsymbol{k}$ as the vibrational number of H_2 molecule increases. These observed features suggest that the degree of the product rotational alignment perpendicular to $\boldsymbol{k}$ displays an increasing-then-decreasing trend over the whole vibrational state. Seen in figure 2(b), as the vibrational state of NH molecule increases, the distribution of $P(\theta_r)$ becomes broader with lower peak position at $\theta_r = 90°$, and this demonstrates that the product alignment becomes weaker at higher vibrational state. The only exceptions are seen for $v = 0$ and $v = 1$, which show no marked differences. Thus, as revealed by the $P(\theta_r)$ distributions of both N(^{4}S) + H_2 → NH + H and its reverse reaction, for high vibrational excitation, the product rotational alignment of both reactions becomes weaker with increase in vibrational quantum number. However, the effect of reagent vibration on the $P(\theta_r)$ distribution in N(^{4}S) + H_2 → NH + H reaction is more evident than that of the reverse NH + H(^{2}S) → N(^{4}S) + H_2 reaction. Since the reaction barrier of N(^{4}S) + H_2 → NH + H is much higher that that of NH + H(^{2}S) → N(^{4}S) + H_2, this phenomenon indicates that, of the two reactive systems, the one with the higher barrier height should have more pronounced reagent vibrational effect on the product alignment perpendicular to $\boldsymbol{k}$. In addition, we

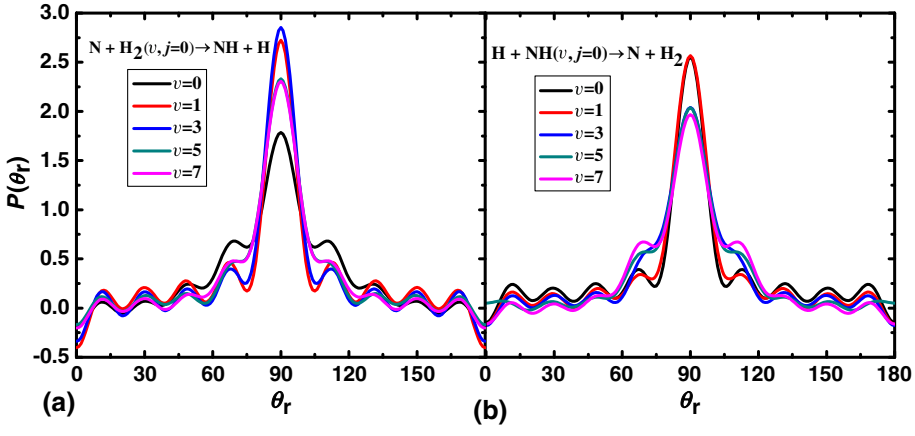

Figure 2. The $P(\theta_r)$ distribution as a function of the angle θ_r between $\boldsymbol{k}$ and $\boldsymbol{j'}$ ($0° \leq \theta_r \leq 180°$) for (**a**) N (^{4}S) + H_2 ($v = 0$, 1, 3, 5, 7, $j = 0$) and (**b**) H (^{2}S) + HN ($v = 0$, 1, 3, 5, 7, $j = 0$).

would like to mention that the abstraction mechanism underlying these two reactions taking place on the $^4A''$ electronic state is different from that of the $N(^2D) + H_2$ reaction on the $^2A''$ electronic state. As known, an insertion mechanism is dominant for the $N(^2D) + H_2$ reaction. For example, this insertion type of mechanism has been vividly shown in the quantum wave packet study of Rao and Mahapatra,[43] where formation of resonances as well as a heavy built-up of probability density near the perpendicular geometry of NH_2 in the time evolution of the decaying resonance indicating that N atom approaches the H_2 molecule perpendicularly, supported the insertion type of reaction mechanism.

The dihedral angle distribution of $\boldsymbol{k} - \boldsymbol{k}' - \boldsymbol{j}'$, in figure 3, shows the degree of the alignment and orientation of $\boldsymbol{j}'$. Clearly, the $P(\varphi_r)$ distribution illustrates asymmetric property with respect to the scattering $\boldsymbol{k}-\boldsymbol{k}'$ plane, with larger distribution peak appearing around $\varphi_r = 270°$. This feature provides the information that both the reactive systems show strong product polarizations and the products tend to be oriented along the negative direction of y-axis. It is noteworthy that $P(\varphi_r)$ distribution for the $N(^4S) + H_2 \rightarrow NH + H$ reaction (see figure 3a) shows a reduction trend as the initial vibrational state increases, thus suggesting that the orientation of the $\boldsymbol{j}'$ vector in the CM frame is weaker at higher vibrational quantum state. In other words, with the vibrational excitation, the preference for in-plane rotation of $\boldsymbol{j}'$ changes to a preference for out-of-plane rotation. A similar finding has also been revealed for the reverse $NH + H(^2S) \rightarrow N(^4S) + H_2$ reaction (see figure 3b). Of the two reactions, reagent vibrational excitation less influences the $P(\varphi_r)$ distribution of the $NH + H(^2S) \rightarrow N(^4S) + H_2$ reaction, since the dihedral angle distributions of the $NH + H(^2S)$ reaction initiated from different vibrational states seem quite similar to each other.

The normal differential cross-section (DCS) describes the $\boldsymbol{k} - \boldsymbol{k}'$ correlation or the scattering direction of the products and is not associated with the orientation and alignment of the product rotational angular momentum vector $\boldsymbol{j}'$. By dividing a factor of $2\pi/\sigma$ from our calculated $PDDCS_{00}$, we obtained DCS under different initial vibrational excitation, as shown in figure 4a and b for the $N(^4S) + H_2 \rightarrow NH + H$ and $NH + H(^2S) \rightarrow N(^4S) + H_2$ reaction, respectively. From figure 4a, it can be seen that the NH products show apparent backward scattering with $v = 0$ and 1. However, product scattering is dominated by the forward and sideways scattering at $v = 3$. At the higher vibrational states of $v = 5$ and 7, the forward scattering is very obvious. A similar situation can be found in figure 4b, where at the ground vibrational state of $v = 0$, the DCS shows a broad backward–sideway distribution, and with increase in the reagent vibrational quantum number, the scattered direction of the products shifts towards the forward direction, with the strongest degree of the forward scattering at $v = 7$. Thus, in both $N(^4S) + H_2 \rightarrow NH + H$ and its reverse reaction, forward scattering becomes stronger with increase in vibrational quantum number. This observed trend in forward scattering can be connected to the PES feature of the $^4A''$ electronic state. Since both the reactions have potential barriers in the entrance channel along their reaction paths, the increment in vibrational quantum number is helpful for the reagents to leap over the barrier and form products that are intensely scattered in the forward direction. In addition, comparing the changes of DCS with initial vibrational excitation in figure 4a and b, we can see that the influence of initial vibrational

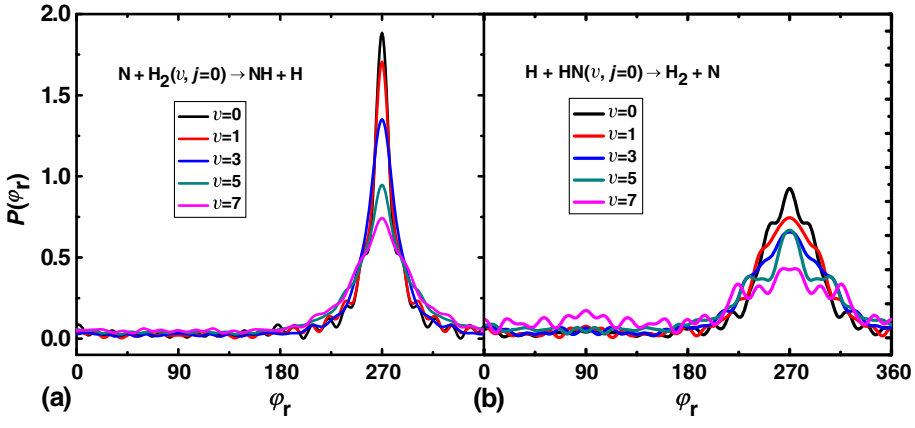

Figure 3. The P (φ_r) distribution as a function of the dihedral angle φ_r ($0° \leq \varphi_r \leq 360°$) for (**a**) N ($^4S$) + H_2 ($v = 0, 1, 3, 5, 7$, $j = 0$) and (**b**) H (^2S) + HN ($v = 0, 1, 3, 5, 7$, $j = 0$).

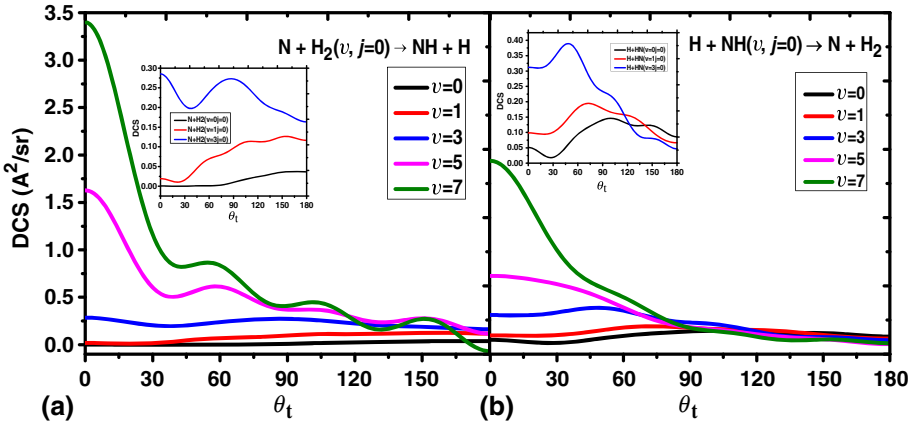

Figure 4. The normal differential cross-sections as a function of the scattering angle θ_t ($0° \leq \theta_t \leq 180°$) for (**a**) N (^{4}S) + H_2 ($v = 0, 1, 3, 5, 7$, $j = 0$) and (**b**) H (^{2}S) + HN ($v = 0, 1, 3, 5, 7$, $j = 0$). The insert panel is a clear demonstration of the cases of $v = 0, 1, 3$, $j = 0$.

excitation on DCS of the NH + H(^{2}S) reaction is rather weaker than that of the N(^{4}S) + H_2 reaction, suggesting that higher the reaction barrier, the more pronounced the vibrational excitation effect on DCS.

3.2 *Effects of rotational excitation on the N(^{4}S) + H_2 and its reverse reaction*

The distributions of $P(\theta_r)$ under different rotational excitation are shown in figure 5 for both N(^{4}S) + H_2 and NH + H(^{2}S) reactions. Similarly, all the distributions have a maximum at $\theta_r = 90°$ and are symmetric with respect to $\theta_r = 90°$, indicating that the product rotational angular momentum is strongly aligned along the direction perpendicular to the relative velocity direction. Inspection of the calculation values in figure 5a and b shows that $P(\theta_r)$ distributions of the N(^{4}S) + H_2 and NH + H(^{2}S) reactions are both broader and lower with the increasing j, which indicates that the degree of alignment of products from the two reactions becomes weaker with initial rotational excitation. Comparing these distributions of the forward reaction with that of the reverse reaction, the $P(\theta_r)$ distribution of the NH + H(^{2}S) reaction changes largely with the quantum number of j, that is to say, $P(\theta_r)$ distribution in NH + H(^{2}S) → N(^{4}S) + H_2 is more sensitive to the reagent rotational excitation than that of N(^{4}S) + H_2 → NH + H.

Figure 6 shows the dihedral angle distributions of $P(\varphi_r)$ at different initial rotational quantum numbers for both reactions. Again, the strong polarization of product rotational angular momentum $\boldsymbol{j'}$ under different rotational excitation is reflected by the fact that the $P(\varphi_r)$ distribution is not asymmetric with respect to the $\boldsymbol{k} - \boldsymbol{k'}$ scattering plane for both reactions. Besides,

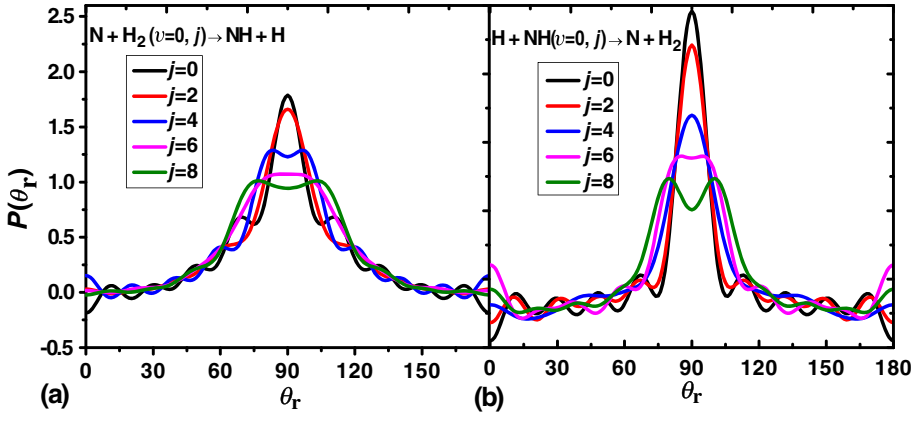

Figure 5. The P (θ_r) distribution as a function of the angle θ_r between $\boldsymbol{k}$ and $\boldsymbol{j'}$ ($0° \leq \theta_r \leq 180°$) for (**a**) N (^{4}S) + H_2 ($v = 0$, $j = 0, 2, 4, 6, 8$) and (**b**) H (^{2}S) + HN ($v = 0$, $j = 0, 2, 4, 6, 8$).

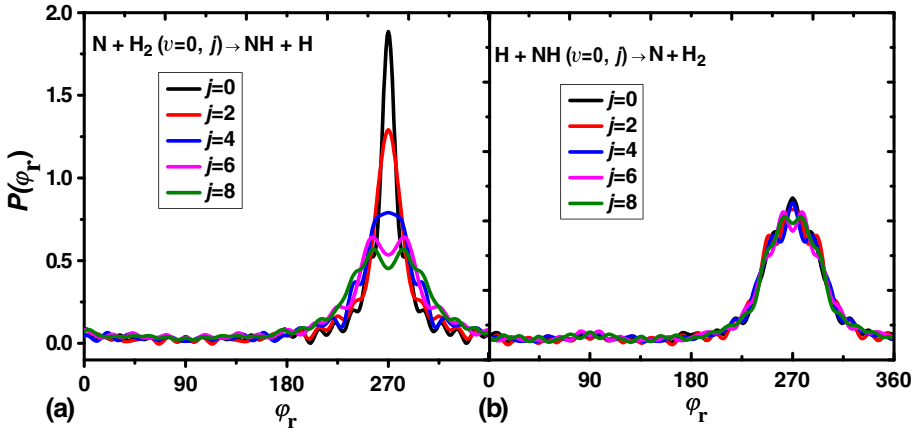

Figure 6. The P (φ_r) distribution as a function of the dihedral angle φ_r ($0° \leq \varphi_r \leq 360°$) for (**a**) N (^{4}S) + H_2 ($v = 0$, $j = 0, 2, 4, 6, 8$) and (**b**) H (^{2}S) + HN ($v = 0$, $j = 0, 2, 4, 6, 8$).

the peak of $P(\varphi_r)$ distribution appears only at $\varphi_r = 270°$, which implies a preference for the left-handed product rotation in planes parallel to the scattering plane. For the N(^{4}S) + H_2 → NH + H reaction, obviously there is weaker product orientation with the increase in rotational quantum number. However, for the NH + H(^{2}S) → N(^{4}S) + H_2 reaction, $P(\varphi_r)$ distributions are almost identical to each other, suggesting a very minor rotational excitation effect on the product rotational polarization. Thus, rotational excitation exerts more significant effect on the product rotational polarization in the N(^{4}S) + H_2 reaction than in the NH + H(^{2}S) reaction.

Figure 7 displays normal DCS with different rotational excitation for the N(^{4}S) + H_2 and NH + H(^{2}S) reactions. The results in figure 7a (for the reaction of N(^{4}S) + H_2) demonstrate that the products are all backward scattered at different rotational excitations. In detail, for $j = 2$, 4 and 6, the degree of the backward scattering decreases with the increment of j, but for $j = 8$, the backward scattering is however reinforced, as compared with that for $j = 0$. The most remarkable feature of the angular distribution shown in figure 7b (for the reaction of NH + H(^{2}S)) is the strong dominance of the broad sideways scattering. Besides, there are some forward and backward peaks, showing a rather complicated structure, and forward-scattering is favoured with low j, while for high j, a preference of backward scattering is visible.

3.3 *Effects of vibrational and rotational excitations on the product alignment parameter* $\langle P_2(j' \cdot k)\rangle$

The average rotational alignment parameter $\langle P_2(\boldsymbol{j'} \cdot \boldsymbol{k})\rangle$, which can be measured in many experiments,

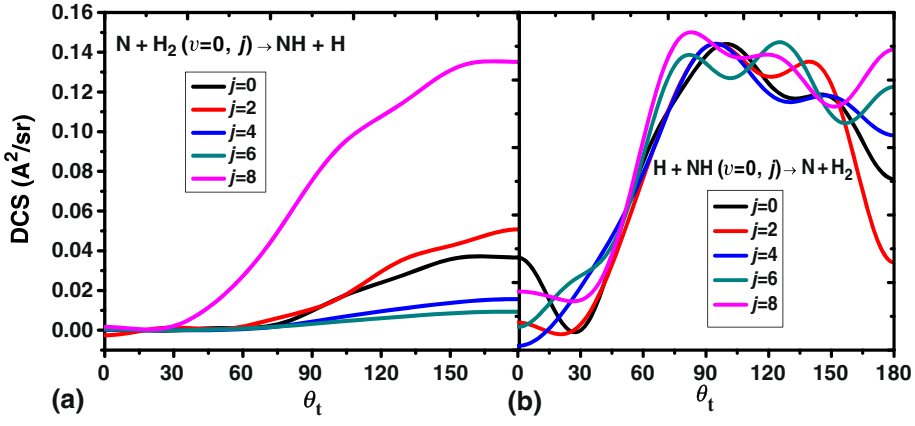

Figure 7. The normal differential cross-sections as a function of the scattering angle θ_t ($0° \leq \theta_t \leq 180°$) for (**a**) N (^{4}S) + H_2 ($v = 0$, $j = 0, 2, 4, 6, 8$) and (**b**) H (^{2}S) + HN ($v = 0$, $j = 0, 2, 4, 6, 8$).

depicts the degree of product alignment quantitatively. Moreover, the calculation of $\langle P_2(\boldsymbol{j'}\cdot\boldsymbol{k})\rangle$ makes it feasible to compare between theory and experiment. From the experimental side, there are a large number of reactions whose parameters are determined. For example, by means of the polarized laser-induced fluorescence (PLIF) of the product, Li *et al.*[21] measured the values of $\langle P_2(\boldsymbol{j'}\cdot\boldsymbol{k})\rangle$ of the product SrBr from the reactions of Sr + CH_3Br, C_2H_5Br, n-C_3H_7Br, i-C_3H_7Br, and found that product alignment becomes less anisotropic with increase in the number of carbon atoms in RBr, which is in good agreement with theoretical calculation results. The product rotational alignment of $\langle P_2(\boldsymbol{j'}\cdot\boldsymbol{k})\rangle = -0.35\pm0.04, -0.15\pm0.02$ was experimentally obtained for CaCl(B), CaCl(A) of the reaction of Ca + NOCl by Zhang *et al.*[28] which is also in good agreement with theoretical results. The experimental data characterizing the angular momentum polarization of the products of the reaction $Cl(^2P_{3/2}) + CD_4(v=0, j=0) \rightarrow DCl(v'=0, j'=1) + CD_3$, is in excellent agreement with the QCT calculated values at a collision energy of 6.46 kcal/mol.[29]

To obtain a better understanding of the product rotational alignment and its relationship with initial vibrational and rotational excitations for the two investigated reactions, we also calculated this expectation value of $\langle P_2(\boldsymbol{j'}\cdot\boldsymbol{k})\rangle$ as a function of vibrational and rotational quantum numbers, and the corresponding results are shown in figure 8. First, it can be seen from figure 8a that the $\langle P_2(\boldsymbol{j'}\cdot\boldsymbol{k})\rangle$ values of both the $N(^4S) + H_2$ and $NH + H(^2S)$ reactions decrease with increment of v, i.e., the product rotational alignment strongly depends on the vibrational quantum number for both reactions. As is known, concerning the product alignment parameter $\langle P_2(\boldsymbol{j'}\cdot\boldsymbol{k})\rangle$, the more the value of this parameter approaches -0.5, the more the product is aligned along the direction perpendicular to $\boldsymbol{k}$. Based on this, both the reactions exhibit stronger product alignment perpendicular to $\boldsymbol{k}$ at high vibrational quantum number. Besides, with increasing v, the $\langle P_2(\boldsymbol{j'}\cdot\boldsymbol{k})\rangle$ values of the $N(^4S) + H_2$ reaction oscillate much while those of the $NH + H(^2S)$ reaction decrease slightly, reflecting that correlation between the initial quantum number v and the product alignment is stronger in the $N(^4S) + H_2$ reaction than the $NH + H(^2S)$ reaction. Second, it can be seen from figure 8b that the $\langle P_2(j'\cdot k)\rangle$ curve of the $N(^4S) + H_2$ reaction shows a decreasing-then-increasing trend as j increases, with the minimum value at $j = 6$, this suggests that the product rotational alignment (perpendicular to $\boldsymbol{k}$) has strong dependence on the rotational quantum number and the strongest product rotational alignment should appear at $j = 6$. However, the $\langle P_2(\boldsymbol{j'}\cdot\boldsymbol{k})\rangle$ values of the $NH + H(^2S)$ reaction are hardly changed with the increment of j, and its minimum value is -0.32, which indicates that the alignment of the products is rather weaker and insensitive to j. Comparison of $\langle P_2(\boldsymbol{j'}\cdot\boldsymbol{k})\rangle$ between the $N(^4S) + H_2$ and $NH + H(^2S)$ reactions, revealed that the $N(^4S) + H_2$ reaction has more negative $\langle P_2(j'\cdot k)\rangle$ value than its reverse one, thus reflecting that the forward reaction exhibits stronger product alignment perpendicular to $\boldsymbol{k}$. To the best of our knowledge, the product alignment of the two reactions has not yet been probed in reactive-scattering experiments at present. Thus, we look forward to the experimental results and fulfill a comparison between theoretical and experimental studies.

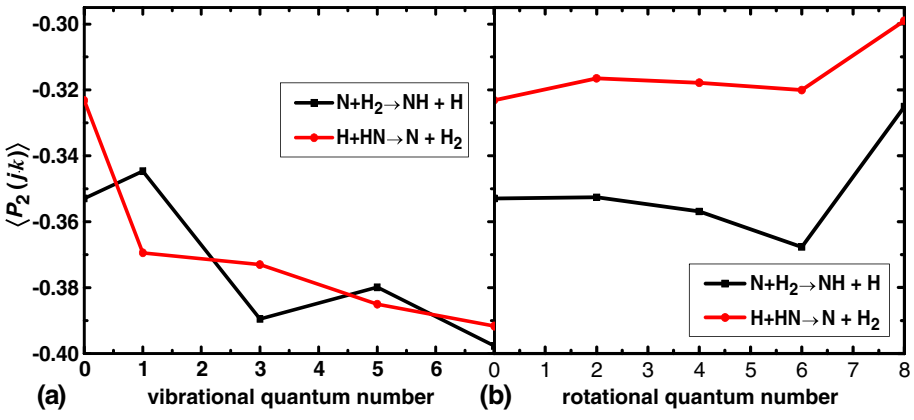

Figure 8. The product rotational alignment of $\langle P_2(j'\cdot k)\rangle$ as a function of the initial (**a**) vibrational and (**b**) rotational quantum numbers for both the $N(^4S) + H_2 \rightarrow NH + H$ and the $H(^2S) + HN \rightarrow H_2 + N$ reactions.

3.4 *Analysis*

Information on stereodynamics of the two reactions has now been obtained and discussed in earlier sections, with different product polarizations for different reagent vibrational and rotational quantum numbers being revealed. Results of the QCT calculation showed that the products not only aligned strongly along the direction perpendicular to the reagent initial relative vector $\boldsymbol{k}$, but also oriented along the direction of the negative y-axis. Further, polarization of the product rotational angular momentum in the $N(^4S) + H_2 \rightarrow NH + H$ reaction is much more sensitive to the vibrational excitation than that of the $NH + H(^2S) \rightarrow N(^4S) + H_2$ reaction. However, the rotational excitation affects the alignment degree of product rotational angular momentum in the $NH + H(^2S) \rightarrow N\ (^4S) + H_2$ reaction more than that of the $N(^4S) + H_2$ reaction, while the opposite situation is seen in the orientation degree of product rotational angular momentum.

For the two reactions, the common phenomena that we have observed are the asymmetric property of the $P(\varphi_r)$ distribution with respect to $\varphi_r = 180°$ and the symmetric property of the $P(\theta_r)$ distribution with respect to $\theta_r = 90°$. The reason behind these phenomena is as follows. According to the impulsive model[21] proposed for the reaction type of A + BC → AB + C, we have $\boldsymbol{j}' = \boldsymbol{L}\sin^2\beta + \boldsymbol{j}\cos^2\beta + \boldsymbol{J}_1 m_B/m_{AB}$, where $\boldsymbol{L}$ and $\boldsymbol{j}$ are the reagents orbital and rotational angular momentum, $\cos^2\beta$ is the mass factor defined by $m_A m_C/(m_A+m_B)(m_B+m_C)$, and $J_1 = a\sqrt{\mu_{BC}R}\ (r_{AB} \times r_{CB})$. Here, u_{BC} is the reduced mass of the BC molecule and $\boldsymbol{r}_{AB}$, $\boldsymbol{r}_{CB}$ are the unit vectors where B points to A and B points to C, respectively; R is the repulsive energy. Starting from the model, when the chemical bond forms and breaks during the reactive processes, $\boldsymbol{L}\sin^2\beta + \boldsymbol{j}\cos^2\beta$ is symmetric, while $\boldsymbol{J}_1 m_B/m_{AB}$ shows a preferring direction because of the repulsive energy and results in the biased orientation of the products.

The reason why vibrational and rotational excitations have a more obvious effect on the product rotational alignment, as reflected by $P(\varphi_r)$, in the $N(^4S) + H_2$ reaction than in the $NH + H(^2S)$ reaction, may be first related to the repulsive energy R of the two reactions. It is conjectured that in the former reaction, the repulsive energy R with initial rovibrational excitation is comparatively greater, which would cause more sensitivity of the product polarizations to the initial vibrational and rotational excitations in the $N(^4S) + H_2$ reaction. The two reactions belong to the reaction type of the heavy–light–light (HLL) mass combination, and according to the pioneering studies[44,45] of Polanyi and coworkers focusing on the reactions of D+HBr and H+DBr with the same type of mass combination, the mass of the attacking atoms and the moment of inertia of the diatom should have influence on alignment effect. They found that alignment effect increases in the reaction with heavy attacking atoms, and low moment of inertia of the diatom. Thus, probably, the more obvious effect of the initial excitation in the $N(^4S) + H_2$ reaction may also be related to the heavier attacking N atom and lower moment of inertia of H_2 molecule, as compared with the $H(^2S)$+NH reaction. The other reason may be related to the different features of the energy profiles along the reaction paths of the two reactive systems. Han *et al.*[20] previously revealed that, for HLL mass combination, the product rotational alignment is independent of the potential barrier location on potential surface. Based on this, we can deduce that the location of the energy barrier does not play an important role in influencing the product alignment for the $N(^4S) + H_2$ and $NH + H(^2S)$ reactions, which also belong to the type of HLL mass combination. Thus, the differences of product rotational alignments may be attributable to the other factor of the barrier height on the potential surface. As we know, on the $^4A''$ DMBE PES, the zero-energy corrected barrier height is 22.5 kcal/mol and 0.8 kcal/mol for the $N(^4S) + H_2 \rightarrow NH + H$ and $H(^2S) + HN \rightarrow H_2 + N$ reaction, respectively. Then, at low vibrational and rotational states of the $N(^4S) + H_2 \rightarrow NH + H$ reaction, the ground-state nitrogen atoms can recoil easily from the hydrogen molecules because of the rather high reaction barrier. However, as the vibrational and rotational states of H_2 molecule increase, it is easy for the reactive system to go through the reaction barrier, thus having clear effect of vibrational and rotational excitations on the product rotational angular momentum in this reactive system with higher barrier height. However, for the $H(^2S) + HN \rightarrow H_2 + N$ reaction with small barrier, the hydrogen atoms easily go through the low energy barrier in the entrance channel whenever the vibrational and rotational states are low or high, causing less sensitivity of the product rotational angular momentum to the reagent vibrational and rotational excitations as compared with the $N(^4S) + H_2 \rightarrow NH + H$ reaction.

4. Conclusion

We have performed a QCT study employing the $^4A''$ DMBE PES of the NH_2 reactive system and explored the influence of the reagent vibrational and rotational excitations on the polarization of product rotational angular momentum for the reactions of $N(^4S) + H_2$ and $HN + H(^2S)$ at a collision energy of 35 kcal/mol. It

has been found that for the two reactions, product rotational angular momentum vectors are not only aligned but also oriented, with more sensitive product polarization to the reagents vibration excitation being found in the $N(^4S) + H_2$ reaction as compared with the $H(^2S)$ + NH reaction. Normal DCS have been presented for different initial rovibrational states. As v increases, the forward scattering becomes stronger and the backward scattering becomes weaker for the two reactions, with stronger v-dependence being revealed for the $N(^4S) + H_2$ reaction. On the whole, the tendencies of the product rotational alignment parameter $\langle P_2(\boldsymbol{j}' \cdot \boldsymbol{k})\rangle$ with initial vibrational excitations are quite similar for the two reactions, showing stronger product alignment perpendicular to $\boldsymbol{k}$ with the increment of v. While concerning the rotational excitation effect, product alignment along the perpendicular direction to $\boldsymbol{k}$ is less sensitive to the reagent rotational excitations in the $N(^4S) + H_2$ reaction than in the NH + $H(^2S)$ reaction, while an opposite situation has been found for the product orientation. Moreover, the products are mainly backward scattered in the $N(^4S) + H_2$ reaction and sideways scattered in the NH + $H(^2S)$ reaction. The values of the calculated $\langle P_2(j' \cdot k)\rangle$ have demonstrated that product alignment is stronger in the $N(^4S) + H_2$ reaction than that of the NH + $H(^2S)$ reaction.

References

1. Kobayashi H, Takayanagi T, Yokayama K, Sato T and Tsunashima S 1995 *J. Chem. Soc.* **91** 3771
2. Umemoto H and Matsumoto K 1996 *J. Chem. Phys.* **104** 9640
3. Pederson L A, Schatz G C, Ho T, Hollebeek T, Rabitz H and Harding L B 1999 *J. Chem. Phys.* **110** 9091
4. Pederson L, Schatz G, Hollebeek T, Ho T-S, Rabitz H and Harding L B 2000 *J. Phys. Chem.* **A104**, 2301
5. Xu Z F, Fang D C and Fu X Y 1997 *J. Phys. Chem.* **A101** 4432
6. Zhang S and Truong T N 2000 *J. Chem. Phys.* **113** 6149
7. Pascual R Z, Schatz G C, Lendvay G and Troya D 2002 *J. Phys. Chem.* **A106** 4125
8. Han B R, Yang H, Zheng Y J and Varandas A J C 2010 *Chem. Phys. Lett.* **493** 225
9. Koshi M, Yoshimura M, Fukuda K, Matsui H, Saito K, Watanabe M, Imamura A and Chen C X 1990 *J. Chem. Phys.* **93** 8703
10. Davidson D F and Hanson R K 1990 *Int. J. Chem. Kin.* **22** 843
11. Adam L, Hack W, Zhu H, Qu Z W and Schinke R 2005 *J. Chem. Phys.* **122** 114301
12. Jordan M J T, Thompson K C and Collins M A 1995 *J. Chem. Phys.* **102** 5647
13. Varandas A J C 2007 *Adv. Chem. Phys.* **74** 255
14. Poveda L A and Varandas A J C 2005 *Phys. Chem. Chem. Phys.* **7** 2849
15. Dunning Jr T H 1989 *J. Chem. Phys.* **90** 1007
16. Yao H B and Zheng Y J 2011 *Phys. Chem. Chem. Phys.* **13** 8900
17. Chu T S 2010 *J. Comput. Chem.* **31** 1385
18. Werner H J and Knowles P J 1988 *J. Chem. Phys.* **89** 5803
19. Knowles P J and Werner H J 1988 *Chem. Phys. Lett.* **145** 514
20. Han K L, He G Z and Lou N Q 1996 *J. Chem. Phys.* **105** 8699
21. Li R J, Han K L, Li F E, Lu R C, He G Z and Lou N Q 1994 *Chem. Phys. Lett.* **220** 281
22. Wang M L, Han K L and He G Z 1998 *J. Phys. Chem.* **A102** 10204
23. Wang M L, Han K L and He G Z 1998 *J. Chem. Phys.* **109** 5446
24. Chen M D, Han K L and Lou N Q 2002 *J. Chem. Phys.* **283** 463
25. Chen M D, Han K L and Lou N Q 2003 *J. Chem. Phys.* **118** 4463
26. Zhang X and Han K L 2006 *Int. J. Quant. Chem.* **106** 1815
27. Han K L, Xu D L, He G Z and Lou N Q 2001 *J. Phys. Chem.* **A105** 2956
28. Zhang J P, Yang H P, Han K L, Deng W Q, He, G Z and Lou N Q 1997 *J. Phys. Chem.* **A101** 7486
29. Zhang L, Chen M D, Wang M L and Han K L 2000 *J. Chem. Phys.* **112** 3710
30. Ju L P, Han K L and Zhang J Z H 2009 *J. Comput. Chem.* **30** 305
31. Aoiz F J, Brouard M, Herrero V J, Saez Rabanos V and Stark K 1997 *Chem. Phys. Lett.* **264** 487
32. Aoiz F J, Brouard M and Enriquez P A 1996 *J. Chem. Phys.* **105** 4964
33. Brouard M, Lambert HM, Rayner S P and Simons J P 1996 *Mol. Phys.* **89** 403
34. Chu T S and Han K L 2008 *Phys. Chem. Chem. Phys.* **10** 2431
35. Chu T S, Zhang Y and Han K L 2006 *Int. Rev. Phys. Chem.* **25** 201
36. J Rao B, Padmanaban R and Mahapatra S 2007 *Chem. Phys.* **333** 135
37. Han K L and He G Z 2007 *J. Photochem. Photobiol. C: Photochem. Rev.* **8** 55
38. Chu T S, Zhang X and Han K L 2005 *J. Chem. Phys.* **122** 214301
39. Xie T X, Zhang Y, Zhao M Y and Han K L 2003 *Phys. Chem. Chem. Phys.* **5** 2034
40. Hu J, Han K L and He G Z 2005 *Phys. Rev. Lett.* **95** 123001
41. Mahapatra S 2004 *Int. Rev. Phys. Chem.* **23** 483
42. Mahapatra S 2009 *Acc. Chem. Res.* **42** 1004
43. J Rao B and Mahapatra S 2007 *J. Chem. Phys.* **127** 244307
44. Hepburn J W, Klimek D, Macdonald R G, Northrup F J and Polanyi J C 1981 *J. Chem. Phys.* **74** 6226
45. Mayne H R and Polanyi J C 1982 *J. Chem. Phys.* **76** 938